Effects of column density on I2 spectroscopy and a determination of I2 absorption cross section at 500 nm

P. Spietz, J. Gómez Martín, J. P. Burrows

Atmos. Chem. Phys., 6, 2177–2191, 2006
www.atmos-chem-phys.net/6/2177/2006/

Atmospheric Chemistry and Physics

Effects of column density on I_2 spectroscopy and a determination of I_2 absorption cross section at 500 nm

P. Spietz, J. Gómez Martín, and J. P. Burrows

Institute of Environmental Physics (IUP), University of Bremen

Received: 15 March 2005 – Published in Atmos. Chem. Phys. Discuss.: 22 July 2005
Revised: 16 December 2005 – Accepted: 24 March 2006 – Published: 20 June 2006

Abstract. The use of ro-vibronic spectra of I_2 in the region of 543 nm to 578 nm as reference spectra for atmospheric Differential Optical Absorption Spectroscopy is studied. It is shown that the retrieval of atmospheric column densities with Differential Optical Absorption Spectroscopy set-ups at FWHM at and above 1 nm depends critically on the column density, under which the used reference spectrum was recorded. Systematic overestimation of the comparatively low atmospheric column density of I_2 of the order of 13% is possible. Under low pressure conditions relevant in laboratory studies, the systematic deviations may grow up to 45%. To avoid such effects with respect to field measurements, new reference spectra of I_2 were determined under column density of the order of 10^{16}cm^{-2} close to that expected for an atmospheric measurement. Two typical configurations of Differential Optical Absorption Spectroscopy, which use grating spectrometers, were chosen for the spectroscopic set-up. One spectrum was recorded at similar resolution (0.25 nm FWHM) but finer binning (0.035 nm/pixel) than previously published data. For the other (0.59 nm FWHM, 0.154 nm/pixel) no previously published spectra exist. Wavelength calibration is accurate to $\pm$0.04 nm and $\pm$0.11 nm respectively. The absorption cross section for the recordings was determined under low column density with an accuracy of $\pm$4% and $\pm$3% respectively. The absolute absorption cross section of I_2 at 500 nm (wavelength: in standard air) in the continuum absorption region was determined using a method independent of iodine vapour pressure. Obtained was $\sigma_{I_2}(500\,\text{nm})=(2.18_6\pm0.02_1)\cdot10^{-18}$ cm^2 in very good agreement with previously published results, but at 50% smaller uncertainty. From this and previously published results a weighted average of $\sigma_{I_2}(500\,\text{nm})=(2.19_1\pm0.02)\cdot10^{-18}$cm^2 is determined.

Correspondence to: P. Spietz
(peterspietz@iup.physik.uni-bremen.de)

1 Introduction

Descriptions of resolution related issues in the ro-vibronic spectrum of I_2 have been reported frequently in the past. Vogt and Koenigsberger (1923) studied the extinction coefficient of iodine vapour in the visible and infrared. They observed strong variation of extinction with temperature, I_2 concentration[1] and foreign gas pressure and reported a clear non-linear behaviour of extinction with respect to concentration – i.e. a deviation from Beer-Lambert's law. Rabinowitch and Wood (1936) determined the transition region between the continuous part of the spectrum below 500 nm and the structured part above 500 nm by varying foreign gas pressure. This left the continuous part of the spectrum unchanged while the structured part changed its apparent extinction significantly. They distinguished clearly between changes due to unresolved rotational lines and effects caused by pressure induced line broadening. Kortüm and Friedmann (1947) recorded the banded region at moderate resolution, relating the observed structure also to the unresolved rotational lines. They also distinguished between pressure induced and concentration induced changes in observed extinction. Ogryzlo and Thomas (1965) proved that the observed pressure dependence of the I_2 absorption spectrum above 500 nm indeed results from pressure broadening of the rotational lines. Tellinghuisen (1973) thoroughly studied the extinction coefficient of I_2 in the visible and NIR under low resolution and resolved the observed spectrum into three transitions $A(^3\Pi_{1u})\leftarrow X(^1\Sigma_{0g+})$, $C(^1\Pi_{1u})\leftarrow X(^1\Sigma_{0g+})$, and $B(^3\Pi_{0u+})\leftarrow X(^1\Sigma_{0g+})$ (see Gray et al., 2001 for labelling of transitions). Today the ro-vibronic spectrum of I_2 is well documented by high-resolution measurements

[1] In some publications the misleading wording "pressure dependence of the I_2 spectrum" was used when relating to I_2 concentration. In the absence of bath gas, $[I_2]$ was varied by varying temperature and thereby vapour pressure. This should not be mixed up with "pressure dependence" resulting from the presence of a foreign gas.

Published by Copernicus GmbH on behalf of the European Geosciences Union.

(Gerstenkorn and Luc 1977a, 1977b, 1978, Gerstenkorn et al., 1982, Kato et al., 2000) and I_2 absorption lines are used as easily accessible wavelength calibration standards (e.g. Marcy and Butler 1992).

But quantitative spectroscopy of I_2 in the said region and under low resolution conditions is still difficult. Because of unresolved ro-vibronic structure each low-resolution spectroscopic measurement is dominated by instrumental artefacts. Under such conditions optical density (OD) is not linear in concentration, when calculated by applying Beer-Lambert's law directly to detector outputs, as in that case the Beer-Lambert's law is applied to arguments, which are not monochromatic intensities (to which the Beer-Lambert law applies), but to convoluted quantities originating from intensities at different wavelengths. Quantitative spectroscopy, which uses low-resolution laboratory spectra of I_2 as reference data, is limited if not impeded by this. Interest in reference spectra of I_2 covering the ro-vibronic region arose (Saiz-Lopez et al., 2004) after the observation of considerable amounts of I_2 in Differential Optical Absorption Spectroscopy measurements (DOAS, see e.g. Perner and Platt (1979), Finlayson-Pitts and Pitts (2000) and Solomon et al. (1987) on zenith sky absorption measurements) in the marine boundary layer at Mace Head, Ireland (Saiz-Lopez and Plane 2004).

With respect to the absorption cross section of I_2 at 500 nm, i.e. outside the ro-vibronic region, a number of studies had been performed in the past. The first determination of the extinction coefficient of I_2 was published by Vogt and Koenigsberger (1923). Other studies followed by Rabinowitch and Wood (1935), Kortüm and Friedheim (1947), Sulzer and Wieland (1952), and Tellinghuisen (1973) establishing the latter's result of $\sigma_{I_2}(500\,\mathrm{nm})=(2.20\pm0.07)10^{-18}\mathrm{cm}^2$ as the most reliable one. Absorption cross section in this context and throughout this text is defined as a molecular quantity of cm^2 per molecule (SI units: cm^2). The recent observation of I_2 in the marine boundary layer by Saiz-Lopez and Plane initiated further studies on the absorption cross section. Studies by Saiz-Lopez et al. (2004) as well as previously unpublished results by Bauer et al. (2004) followed yielding $(2.29\pm0.27)\ 10^{-18}\mathrm{cm}^2$ and $(2.25\pm0.09)\ 10^{-18}\mathrm{cm}^2$ respectively. In recent laboratory studies on the determination of absorption cross sections of iodine oxides as well as related kinetics studies (e.g. EU Framework 5 Program THALOZ) the knowledge of the absorption cross section of I_2 is an important prerequisite to any quantitative analysis adding further to the newly increased interest in I_2.

Both issues, quantitative spectroscopy for DOAS with typical low resolution and the absolute absorption cross section of I_2 at 500 nm are being addressed in this work.

2 Reference spectra of I_2 or DOAS

Due to the measurement process performed with a moderately resolving spectrometer and a semi-conductor detector array, any measurement of unresolved rotational lines will be dominated by instrumental artefacts. One reason for this is the unresolved irregular distribution and mixing of strongly absorbing and absorption free spectral sections within the low-resolution recording. The instrumental artefacts will be a non-linear function of column density (the product of geometric path length and concentration). Likewise such measurements are prone to contain *saturated* rotational lines, i.e. lines which are too strong to allow any measurable intensity to pass at their specific wavelength. This is especially true of laboratory measurements in which it is tempting to use optical densities of the order of 0.5 to 1.0 to improve the signal to noise ratio. Already at I_2 vapour pressure (room temperature) and a path length of 10 cm a large number of I_2 rotational lines between 510 nm and 560 nm are at optical densities above 3. If the Beer-Lambert law is directly applied to the detector output of measured intensities, an apparent optical density A_{app} will be obtained, which is not linear in concentration. Fig. 1a shows two spectra recorded at significantly different column densities under otherwise constant conditions. Resolution was low and rotational lines were far from being resolved. In the continuum range below 500 nm the low column density spectrum is scaled to the high column density one. In the ro-vibrational region the apparent optical density A_{app} clearly grows sub-linearly with column density. Opposed to that optical density at and below 500 nm is continuous and therefore perfectly linear in column density. In the following Sect. 2.1 firstly the effect of resolution and binning on low-resolution recordings of the I_2 ro-vibronic spectrum will be studied. As a consequence from the findings in the simulation section new reference spectra for I_2 were recorded to be used in atmospheric DOAS retrieval. The experiments and the analysis leading to these new reference spectra are presented in Sect. 2.2.

2.1 Simulations

Spectra were simulated based on a high-resolution spectrum of I_2 obtained with a Fourier Transform Spectrometer (FTS), courtesy of Marcy and Butler (1992). Conditions for this high-resolution spectrum are specified as signal to noise S/N=1000, resolution $\lambda/\Delta\lambda$=400 000 ($\approx0.04\mathrm{cm}^{-1}$), $[I_2]$ at vapour pressure (room temperature) without bath gas and 10 cm optical path. A section of this spectrum is shown in Fig. 1b. Clearly a considerable number of lines already reaches OD of the order of 2 to 3. In the lack of other high-resolution data recorded under lower OD and given the large signal to noise ratio of that measurement, this spectrum was nevertheless used as the "true" spectrum in our simulations. The spectrum was convoluted with a $0.3\,\mathrm{cm}^{-1}$ Lorentz profile to simulate atmospheric pressure broadening (estimate

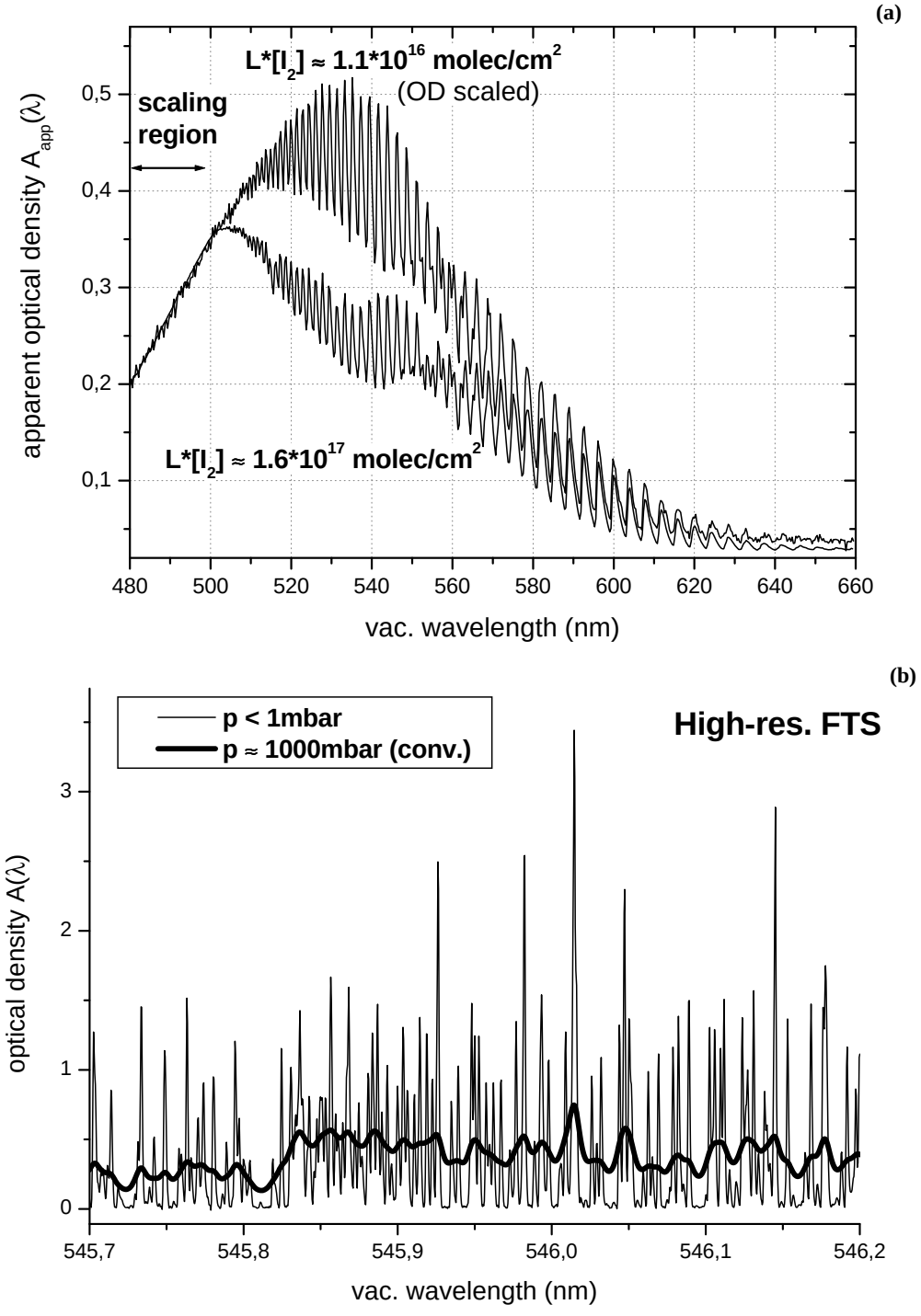

Fig. 1. (a) Two low resolution absorption spectra of I_2 were recorded at significantly different column densities. The low column density spectrum was scaled to the other in the continuum region at $\lambda < 500$ nm. In the ro-vibronic region above 500nm the high column density measurement shows clear sub-linear growth with column density. **(b)** A section of the high-resolution absorption spectrum of I_2 obtained from Fourier Transform Spectrometer measurements is shown ($\approx 0.04\,\mathrm{cm}^{-1}$), courtesy of Marcy and Butler (1992). To simulate atmospheric pressure broadening, the spectrum was convoluted with a $0.3\mathrm{cm}^{-1}$ Lorentz profile (bold line).

Table 1. Spectra were simulated for different spectroscopic configurations. The effect on $\Delta\sigma_{app}$ is based on an atmospheric column density $\approx 4.6{\cdot}10^{15}$cm^{-2} and a reference spectrum recorded at $\approx 4.6{\cdot}10^{17}$cm^{-2}. Atmospheric column density would be overestimated by up to 13%. Configurations A, C, and D are typical atmospheric DOAS configurations. Especially the results for A and B indicate that not binning (measured as FWHM/$\Delta\lambda$) but resolution (FWHM) is the major source of this effect.

config.	grating [grves·mm^{-1}]	$\Delta\lambda$ [nm/pixel]	FWHM [nm]	FWHM/$\Delta\lambda$ [pixel]	effect on $\Delta\sigma_{app}$	reference
A	1200	0.035	0.175	5	−2%	Saiz-Lopez & Plane (2004)
			(0.25)	(7.1)		this work
B	600	0.077	0.35	4.5	−5%	
C	600	0.077	1.0	13.0	−12%	Aliwell & Jones (1997)
D	300	0.154	1.3	8.4	−13%	Richter (1997)

based on comparable air broadened half width in Rothman et al., 2004). This curve is also shown in Fig. 1b. An FTS recording of a Xenon lamp obtained at 2 cm^{-1} resolution was interpolated onto the grid of the I_2 spectrum to be used as the reference intensity $I_0(\lambda)$. With these three data sets low resolution and coarsely binned apparent optical densities A_{app} were then simulated under different spectroscopic conditions defined by different FWHM of the (gaussian shaped) instrument's function, different linear dispersion and different spectral width of the detectors pixels. Spectroscopic conditions were chosen such that they also cover spectroscopic configurations of currently used DOAS instruments (Roscoe et al., 1999 and references therein), see Table 1. The high-resolution I_2 absorption spectra (low pressure and pressure broadened) were scaled to different amplitudes simulating differently strong true optical densities $A_i(\lambda)$. The change in peak height caused by pressure broadening was taken into account. Thereby quantitative comparability was maintained. Applying the Beer-Lambert law, the different absorption measurements $I_i(\lambda)$ were simulated:

$$I_i(\lambda) = I_0(\lambda) \cdot \exp[-A_i(\lambda)] \quad (1)$$

Limited spectral resolution was simulated by convoluting both $I_i(\lambda)$ and $I_0(\lambda)$ with a gaussian shaped instrument's characteristic function $S(\lambda)$. The resulting $I_{c,i}(\lambda)$ and $I_{c,0}(\lambda)$ were then binned (numerically integrated) onto a grid of pixels of fixed size (continuous $\lambda \rightarrow$ discrete j) and from the binned signals $I_{c,i}(j)$ and $I_{c,0}(j)$ an apparent optical density $A_{app,i}(j)$ was calculated:

$$A_{app,i}(j) = \ln\left(\frac{I_{c,0}(j)}{I_{c,i}(j)}\right) = \ln\left(\frac{\int_{\lambda_j}^{\lambda_{j+1}}\int_{-\infty}^{+\infty} S(u)\cdot I_0(\lambda-u)\,du\cdot d\lambda}{\int_{\lambda_j}^{\lambda_{j+1}}\int_{-\infty}^{+\infty} S(u)\cdot I_0(\lambda-u)\cdot\exp(-A_i(\lambda\text{-}u))\,du\cdot d\lambda}\right) \quad (2)$$

This use of apparent optical density is the same as in the study by Tellinghuisen (1973), who tackled the problem in terms of apparent extinction. The peak amplitude of true optical density $A_i(\lambda)$ was varied such that it covered a range of column densities from $\approx 1.8{\cdot}10^{15}$cm^{-2} to $6.4{\cdot}10^{17}$cm^{-2} relevant for field (low end, compare Saiz-Lopez and Plane 2004) and lab (high end). For comparison, room temperature saturated vapour pressure of I_2 at 50cm path length produces a column density of the order of $5{\cdot}10^{17}$cm^{-2}.

3 Results from simulated data

The comparison of the simulated spectra shows that the pressure broadened spectra grow faster in apparent OD than do the low pressure spectra, perfectly in line with the observations of e.g. Rabinowitch and Wood (1935). The faster increase is caused by redistribution of absorption from the line centres to the gaps between lines, compare Fig. 1b. The same as for apparent OD as such is also true for the amplitude of differential structures in the apparent OD spectrum, see Figs. 2a and b. To detect any non-linear behaviour of apparent OD with respect to column density (i.e. the product of concentration and path length), one can either plot apparent OD at a selected wavelength against column density as independent variable. Or one normalises apparent OD to column density and checks, whether the result, i.e. apparent absorption cross section, is constant. Both types of representation will be used below. As DOAS relies upon differential spectra of apparent OD – designated by $\Delta A_{app}(\lambda)$ –, these were extracted by subtracting a suitable slowly varying polynomial from $A_{app}(\lambda)$ and then normalising the resulting $\Delta A_{app}(\lambda)$ to column density to obtain differential cross section $\Delta\sigma_{app}(\lambda)$. In the absence of non-linear effects the differential cross section $\Delta\sigma(\lambda)$ would be independent of column density. But as non-linear effects can not be neglected, $\Delta\sigma_{app}(\lambda)$ is not independent of column density and has therefore to be considered as an apparent quantity. The results for a selected band (546 nm) and two different pressures are shown in Fig. 2a

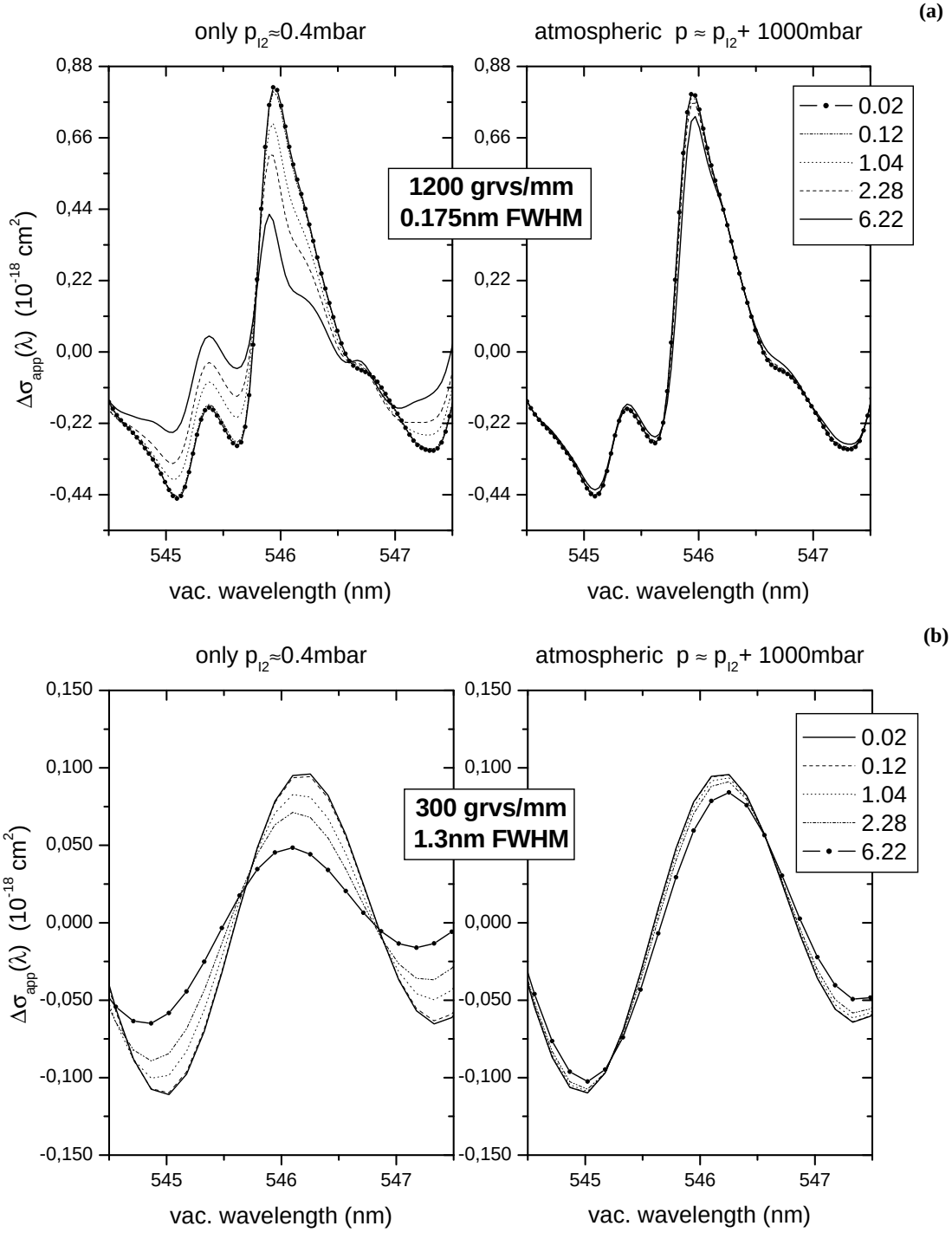

Fig. 2. **(a)** Based on the high-resolution FTS spectrum of I_2 the apparent differential absorption cross sections $\Delta\sigma_{app}$ were simulated for different column densities of I_2 (legend: column density in units of 10^{17} cm^{-2}). Shown is the effect on the 546 nm band at low pressure (left, only I_2) and atmospheric pressure (right: I_2 plus 1000 mbar of bath gas). Increased column density systematically reduces the amplitude of $\Delta\sigma_{app}$. The effect is smaller at atmospheric pressure and large at low pressure. **(b)** Same as Fig. 2a but for 300 grooves·mm^{-1} and 1.3 nm FWHM. Legend: Column density in units of 10^{17}cm^{-2}. Structures are much more smoothed and the amplitude is reduced relative to the 1200 grooves·mm^{-1} grating spectrum.

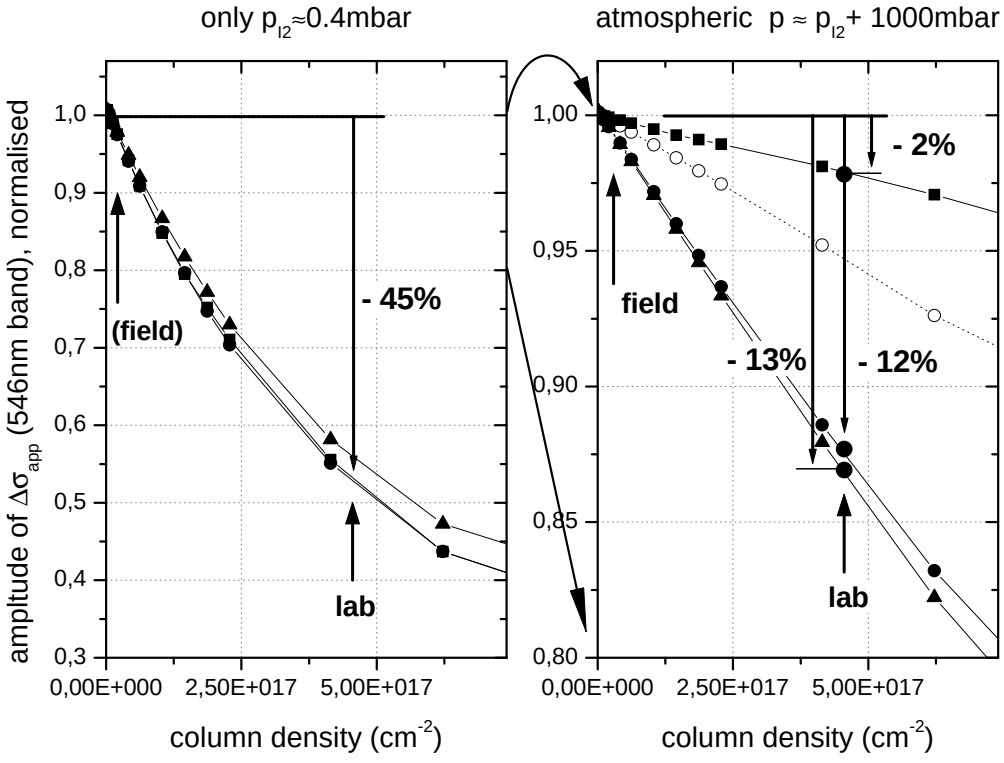

Fig. 3. The amplitude of apparent differential absorption cross section of the 546 nm band was simulated for different spectroscopic conditions (filled squares: 1200 grvs/mm, 0.175 nm FWHM, filled circles: 600 grvs/mm, 1.0 nm FWHM, filled triangles: 300 grvs/mm, 1.3 nm FWHM, open circles: 600 grvs/mm, 0.35 nm FWHM), different column densities (horizontal axis) and two cases of pressure (panels left and right). Data is normalised to recently observed atmospheric column density of I_2 ("field"). $\Delta\sigma_{app}$ is reduced leading to an overestimation of column density of up to 13% (atmospheric case).

for a 1200 grooves·mm^{-1} grating at 0.175 nm FWHM and in Fig. 2b for a 300 grooves·mm^{-1} grating at 1.3 nm FWHM, both being currently used DOAS configurations. The effects of column density on $\Delta\sigma_{app}(\lambda)$ are clearly visible, even though the effect is smaller in the pressure broadened case. The deviation from constant behaviour was quantified by firstly measuring the amplitude of differential structure from valley to peak. This amplitude was then plotted against column density (Fig. 3). Compared were two column densities of $\approx 4.6 \cdot 10^{15}$cm^{-2} and $\approx 4.6 \cdot 10^{17}$cm^{-2}, the lower one corresponding to the order of magnitude observed at the 8.4 km long path DOAS measurement at Mace Head reported by Saiz-Lopez and Plane (2004). The larger one corresponds to a laboratory measurement at room temperature and saturated vapour pressure of I_2 and 50 cm path length. The comparison yielded the relative changes indicated in the figure. Both at low as well as at atmospheric pressure the amplitude of apparent differential cross section is noticeably reduced by increasing column density. If a high column density reference spectrum from the lab were used for DOAS retrieval of low column densities, the latter would be overestimated correspondingly. In the pressure broadened atmospheric case overestimation amounts to 2%, 12% and 13% for 1200 grooves·mm^{-1}, 0.175 nm FWHM (filled squares), 600 grooves·mm^{-1}, 1.0 nm FWHM (filled circles) and 300 grooves·mm^{-1}, 1.3 nm FWHM (filled triangles) respectively. Even though uncertainties in atmospheric retrieval of I_2 are currently dominated by effects of unknown inhomogeneous distribution of I_2 rather than by the spectroscopic effects discussed here, the magnitude of spectroscopic effects is nevertheless sufficiently substantial to justify their consideration. In the low pressure case overestimation reaches 45% and is quite independent of spectroscopic conditions. Use of DOAS in low pressure laboratory studies therefore requires great care in selecting an appropriate reference spectrum. A simulation for 600 grooves·mm^{-1}, 0.35 nm FWHM (Fig. 3, pressure broadened case, open circles) was also performed to examine the source of the observed effect (Table 1). Comparing FWHM as well as the ratio of FWHM upon $\Delta\lambda$ to the observed effect on $\Delta\sigma_{app}$ (esp. configurations A and B) shows that not binning – more precisely the number of pixels covering a spectral feature – but resolution expressed by FWHM is the major source of the effect. This result can give an orientation what to expect, but it can not be generalised, as the effect on $\Delta\sigma_{app}$ is not the same in each band, see Fig. 4. There the reduction of

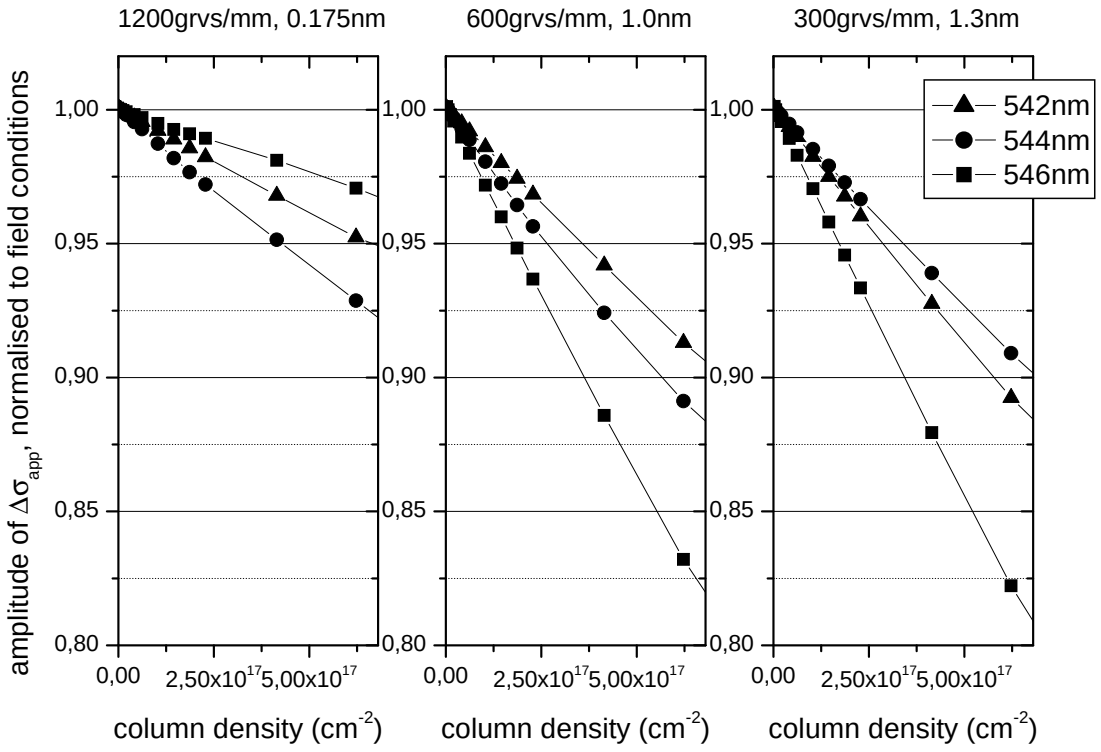

Fig. 4. Sensitivity of different bands to effects of resolution and binning was studied. The amplitude of $\Delta\sigma_{\text{app}}$ was determined at different bands and different spectroscopic conditions (same normalisation as in Fig. 3). It is plotted against column density of I_2 (units: cm^{-2}). Clearly sensitivity to resolution is different in different bands. Note the partially mixed order of results obtained from different bands under different conditions.

$\Delta\sigma_{\text{app}}$ is plotted for three different bands (542 nm, 544 nm, and 546 nm). Note the partially mixed order of curves indicating differently strong and partially reversed effects for different spectroscopic conditions. This different behaviour of $\Delta\sigma_{\text{app}}$ in different bands presents a further problem, if reference spectra recorded at high column density were to be used for DOAS retrieval of low atmospheric column densities. The found overestimation can be minimised by using reference spectra recorded in the range of column density expected in the DOAS application. But it has to be kept in mind that the found effects also dependent on instrument characteristics defined by the instrument's characteristic function $S(\lambda)$ and the pixel size used for numeric integration (binning).

Therefore the best approach is to dedicatedly measure I_2 reference spectra with the DOAS instrument itself in the lab at a column density which is similar to those expected in the atmosphere. If the DOAS instrument itself cannot be used, the second best solution is to use a spectrometer and detector of same type and under the same spectroscopic conditions as later in the atmospheric measurement. In this sense – given the available equipment in our lab – the spectra presented below were measured. With the two aspects "spectroscopic conditions" and "atmospheric target column density" taken into account, overestimation introduced by insufficient resolution will be minimised to 1% or even less, see Fig. 3.

4 Method for largely varying column densities

If an absorber's apparent spectrum should display significant variation already on the scale of column densities expected in the atmosphere (which is not the case for I_2), a single reference spectrum "centred" in the middle of the expected range does not suffice. Rather the expected range has to be covered by a set of reference spectra $\Delta\sigma_{\text{app}}(\lambda,C_j)$ recorded at different column densities C_j. These $\Delta\sigma_{\text{app}}(\lambda,C_j)$ have to be fitted by a polynomial determined at each wavelength λ to enable interpolation of $\Delta\sigma_{\text{app}}(\lambda,C)$ for arbitrary column densities C:

$$\Delta\sigma_{\text{app}}(\lambda, C) = \sum_{k=0}^{m} a_k(\lambda) \cdot C^k \tag{3}$$

The variable of this polynomial is column density C. The coefficients $a_k(\lambda)$ are determined to fit the discrete set of $\Delta\sigma_{\text{app}}(\lambda, C_j)$. Instead of a simple differential reference spectrum $\Delta\sigma_{\text{app}}(\lambda)$ now the wavelength dependent coefficients $a_k(\lambda)$ contain the information about the reference spectrum plus the instrumental and column density dependent effects.

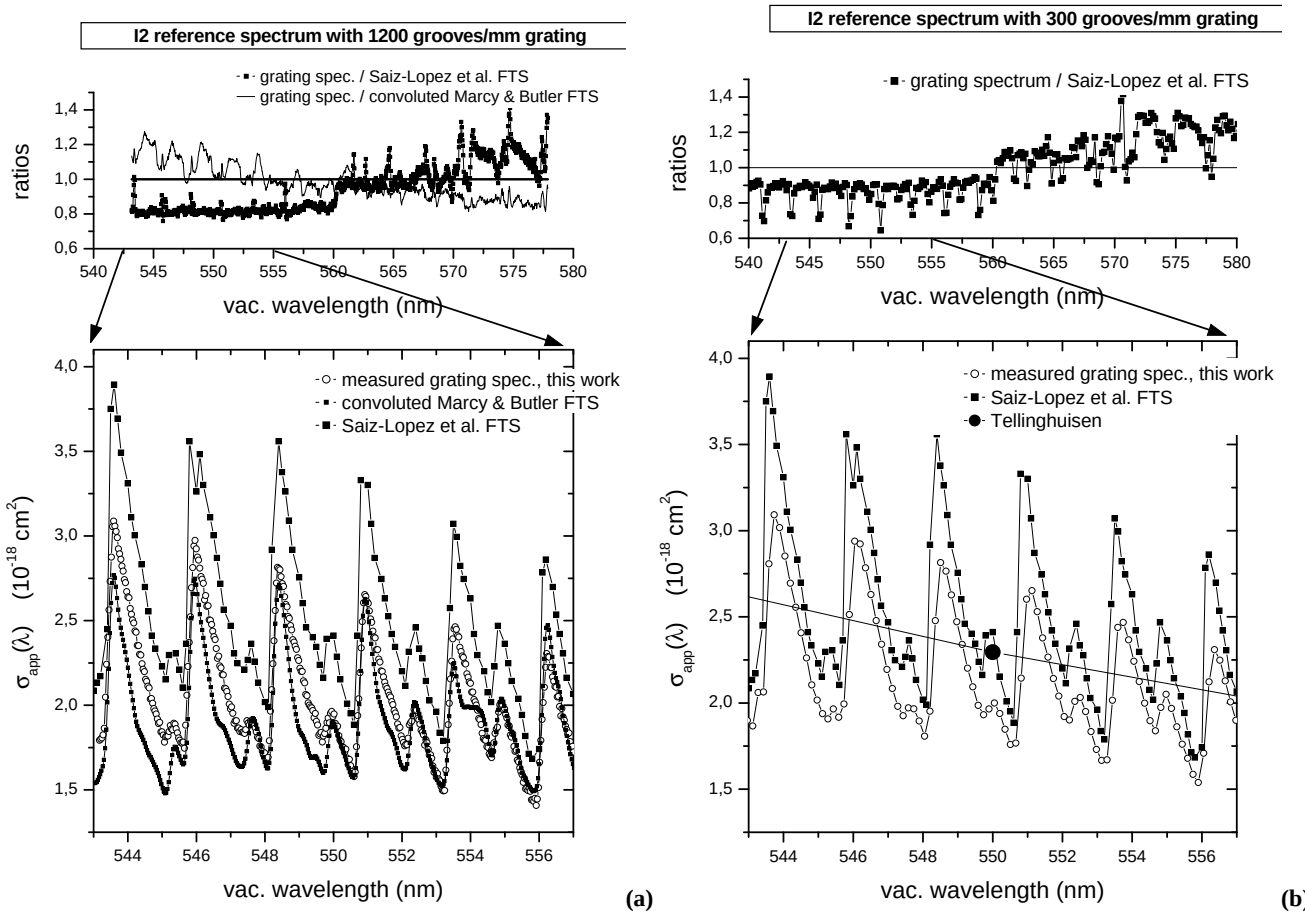

Fig. 5. (a) The spectrum obtained in this work with a 1200 grooves·mm^{-1} grating and 0.25 nm FWHM is compared to a spectrum based on the high-resolution data shown in Fig. 1 simulated for the same spectroscopic conditions as well as to an FTS spectrum obtained by Saiz-Lopez et al., (0.1 nm step size, 4 cm^{-1} resolution). In the top graph the ratio between our measurement and the latter two compares the systematic deviations between the different spectra. **(b)** Same as in Fig. 5a, but for the spectrum obtained with a 300 grooves·mm^{-1} grating and 0.59 nm FWHM. The general behaviour of the ratio is the same as between the 1200 grooves·mm^{-1} grating and the FTS spectrum by Saiz-Lopez. The low-resolution data by Tellinghuisen (1973, monochromator: trapezoidal slit function, 2.9 nm base, 2.3 nm peak width) is also plotted for comparison (filled circle).

4.1 Measurement of reference spectra

To obtain I_2 reference spectra for DOAS, absorption spectra were measured at 1000 mbar (N_2 grade 4.8 added) with the set-up to be described below. The only difference was in that measurements were performed in flow mode using a different iodine reservoir. This enabled either a flow of N_2 through the iodine reservoir or bypassing it. Thereby pressure and flow in the vessel could be maintained constant between reference intensity and absorption intensity measurements. Two spectroscopic configurations were used: Firstly a 300 grooves·mm^{-1} grating and 50 μm slit width ($\rightarrow$ 0.59 nm FWHM, 0.154 nm/pixel) covering the interval from 445 nm to 600 nm. This enabled direct determination of apparent cross section in the ro-vibronic range, as the continuous part of the absorption at 500 nm could be used for determination of concentration. At 500 nm the absolute absorption cross section of $\sigma_{I_2}(500\,\text{nm})=(2.19\pm0.02)\text{cm}^2$ determined in this work (see below) was used.

A second reference spectrum was recorded with a 1200 grooves·mm^{-1} grating and 170 μm entrance slit ($\rightarrow$0.25 nm FWHM, 0.035 nm/pixel) covering the range from 543 nm to 578 nm (560 nm centre wavelength). This corresponded to the conditions in Saiz-Lopez and Plane (2004). There, atmospheric measurements were made with an identical spectrometer as in this study (Acton Research 500 mm Czerny-Turner spectrograph). With the narrow spectral window of the 1200 grooves·mm^{-1} grating absolute calibration of apparent differential cross section was achieved by additional measurements before (index "b") and after (index "a"), which were centred at 500 nm. Measurements were performed in the

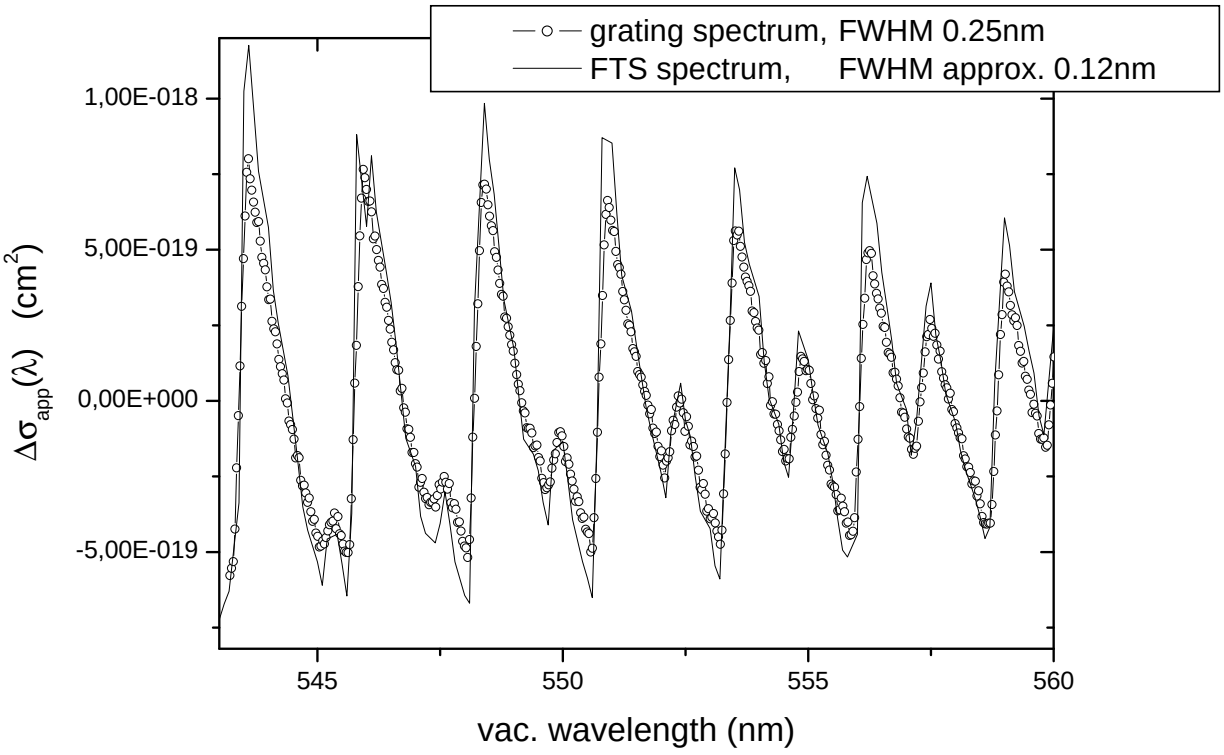

Fig. 6. A spectrum of I_2 was recorded with a 1200 grooves·mm^{-1} grating spectrometer at 0.25 nm FWHM and low column density of $6.9 \cdot 10^{15}$cm^{-2} (open circles). It is compared to an FTS spectrum recorded at somewhat larger column density $3.1 \cdot 10^{16}$cm^{-2}, 0.1 nm step size, 4 cm^{-1} resolution corresponding to approx. 0.12 nm FWHM at 550 nm (solid line). Effects due to different column density are minor. The disagreement in differential amplitude is most likely due to different resolution.

order $I_{0,560\,nm,b}(\lambda)$, $I_{0,500\,nm,b}(\lambda)$, $I_{500\,nm,b}(\lambda)$, $I_{560\,nm}(\lambda)$, $I_{500\,nm,a}(\lambda)$, $I_{0,500\,nm,a}(\lambda)$, and $I_{0,560\,nm,a}(\lambda)$. During the three absorption measurements of $I_{500\,nm,b}(\lambda)$, $I_{560\,nm}(\lambda)$, and $I_{500\,nm,a}(\lambda)$ concentration of $[I_2]$ was maintained constant in the vessel. Between the intensity references $I_{0,560\,nm,b}(\lambda)$ and $I_{0,560\,nm,a}(\lambda)$ and the middle absorption measurement $I_{560\,nm}(\lambda)$ the spectrometer had to be moved for each of the 500 nm measurement blocks. Errors due to this were negligible, because the uncertainty in reproducibility of spectrometer position was better than 0.03 nm. This is small with respect to the in the region 543 nm to 578 nm smooth and slowly varying spectrum of the Xenon arc lamp, which was used in these experiments. By the described procedure absolute calibration of concentration was transferred from 500 nm to the apparent optical density spectra in the structured region.

Wavelength calibration was obtained by recording the emission spectrum of a line source (Platinum-Chromium-Neon and Mercury-Cadmium). Calibration was checked and improved by calibrating the measured spectrum against the convoluted high-resolution FTS spectrum from Marcy and Butler. This had a wavelength accuracy of better than 0.001 nm (corresponding to 0.04 cm^{-1} resolution as upper limit of wavelength accuracy). In the calibration of the I_2 spectrum measured with the 1200 grooves·mm^{-1} grating, eight band maxima of I_2 distributed evenly across the spectral range were used. The mean error of calibration ranged between 0.02 nm and 0.04 nm setting the uncertainty to $\pm$0.04 nm. The same procedure was used for the measurement recorded with the 300 grooves·mm^{-1} grating. 33 band maxima distributed across the interval from 510 to 580 nm were used. The mean error of calibration ranged between 0.03 nm and 0.11 nm setting the uncertainty to $\pm$0.11 nm. FWHM was determined from the apparent shape of isolated emission lines from the mercury-cadmium line source.

5 Resulting spectra

A section of the I_2 reference spectrum obtained for the 1200 grooves·mm^{-1} measurement is shown in Fig. 5a. Also shown are the simulated spectrum based on the FTS data from Marcy and Butler (1992) and the FTS spectrum measured by Saiz-Lopez et al. (2004), to our best knowledge the only other I_2 reference spectrum published for use in DOAS. For comparability the latter is scaled to the cross section at 500 nm of $(2.19\pm0.02)\cdot10^{-18}$cm^2 as determined in this work.

Transfer of concentration from 500 nm was accomplished with an uncertainty of about 4%, which was estimated by comparing empty vessel measurements "before" and "after" and which was confirmed by comparing spectra obtained from different series of spectra. The signal to noise ratio in our spectrum is of the order of 70:1 determined from a ratio of two independent measurements. In the centre region around 562 nm all three spectra coincide well, compare the ratios of spectra, top graph of Fig. 5a. But the general pattern of ratios displays reversed inclination for the two cases with a crossing point at the centre. While the ratio with the simulated spectrum (convoluted Marcy and Butler) continues smoothly with regular differential structures, the ratio with the FTS spectrum by Saiz-Lopez shows a clear jump near the centre and surprisingly different differential structure in the two halves of the considered interval. Band correlated structures coincide systematically with the top and bottom of the steep blue flanks of the bands and reach up to 10%. In the FTS spectrum itself effects of step size (0.1 nm) are clearly visible, where band heads are levelled off and flanks appear bent and irregular (picket-fence effect, see e.g. Bergland 1969). The grating spectrum displays regular flanks and clear band heads, in general agreeing better with the smooth shape and amplitude of the simulated spectrum.

Figure 5b shows the spectrum obtained with a grating of 300 grooves·mm^{-1}. No transfer of calibration was necessary, as λ=500 nm was included in the spectral interval. Three series of at least 10 spectra each were recorded. Effects of deposit on the windows and light source drift were corrected. The scatter between the spectra was of the order of a few percent, which is too small to cause non-linear effects in OD. Therefore all were scaled at 500 nm to the I_2 cross section determined below. From their scatter in differential structure (2.5%) and the uncertainty in cross section the uncertainty of the spectrum is conservatively estimated as 3%. Signal to noise was determined at λ<500 nm to be of the order of 50:1.

The ratio between the 300 grooves·mm^{-1} spectrum and the FTS spectrum by Saiz-Lopez et al., shows the same general pattern as the ratio of the 1200 grooves·mm^{-1} grating spectrum and their FTS spectrum. Band correlated structures are larger and at the same positions as above.

5.1 Discussion and conclusion

With respect to the inclination of ratios it is interesting to note that to the blue side of the observed turning point the $C(^1\Pi_{1u})\leftarrow X(^1\Sigma_{0g+})$ and $B(^3\Pi_{0u+})\leftarrow X(^1\Sigma_{0g+})$ transitions are relevant while to the red the $A(^3\Pi_{1u})\leftarrow X(^1\Sigma_{0g+})$ becomes dominant (compare Tellinghuisen 1973 and Gray et al., 2001). This explains the inclination of the ratio with respect to the simulated spectrum, as the original Marcy and Butler FTS spectrum was obtained without intensity reference measurement. Any smooth continuous absorption including the continuous $C(^1\Pi_{1u})\leftarrow X(^1\Sigma_{0g+})$ transition was therefore lost in the calculation of OD from their data. The simulated spectrum therefore has to fall below any measured spectrum. The remaining deviation from a ratio of 1.0 could be caused by inaccurate scaling of the simulated spectrum. This was determined iteratively and only roughly as the main purpose was comparison among the simulated spectra. The differential structures in the ratio follow the pattern of the ro-vibrational bands and are likely due to oversimplification of the instrument's function in the simulation process (gaussian). The same is true of the artificial pressure broadening with a Lorentz profile of idealised fixed width. Apart from that, strong and possibly saturated lines present in the original Marcy and Butler data could be responsible as well.

The deviations in the ratio between our spectra and that by Saiz-Lopez et al., are less easily understood (compare also Fig. 6). It is important to note, that the general pattern of the ratio is the same for the 1200 grooves·mm^{-1} and the 300 grooves·mm^{-1} grating spectrum, which were obtained in different sets of experiments. At first sight the observed behaviour could indicate a – for technical reasons necessary joining of different sections of FTS recordings near 560 nm. But this is not the case, as the different sections were joined by linear weighting from 500 to 555 nm (Saiz-Lopez, private communication). The column density in the recording of their FTS spectrum was $3.1\cdot10^{16}$cm^{-2}, which is only a factor of 4.5 larger than in our measurements. This excludes column density dependent effects as well. Rather different resolution and possibly light source drift or deposit causing broad band changes of throughput are likely to explain the observed discrepancies. Resolution in our spectrum (Fig. 5b) was at 0.25 nm FWHM. In the FTS recording it was a factor of two smaller at 4 cm^{-1}, which at 550 nm corresponds to 0.12 nm. This is nearly the same as the chosen step size of 0.1 nm in their spectrum, explaining the observed picket fence effect in their spectrum. While comparability is somewhat limited by different resolution and step size, the presented spectra are in reasonable agreement with the FTS spectrum by Saiz-Lopez et al. Consistency of our measured and simulated spectra supports the validity of the conclusions drawn from the simulations. For measurements with 1200 grooves·mm^{-1} grating and FWHM of 0.175 nm no significant problems have to be expected from different column density. But in other spectroscopic configurations at low resolution, i.e. FWHM of 1.0 nm and above, the effects by different column density become significant. This justifies dedicated measurements of reference spectra at target column density and with the DOAS instrument itself or at least with the same type of instrument. As the effect of column density in such cases is of the order of somewhat more than 10%, an approximate knowledge of the target optical density can be obtained by neglecting this effect. In a second step the improved reference spectra at target column density can then be determined to improve the atmospheric retrieval. The two absorption spectra presented in this work were both measured under column densities of the order of 10^{16} cm^{-2} which according to Saiz-Lopez and Plane (2004) is close to those expected in the

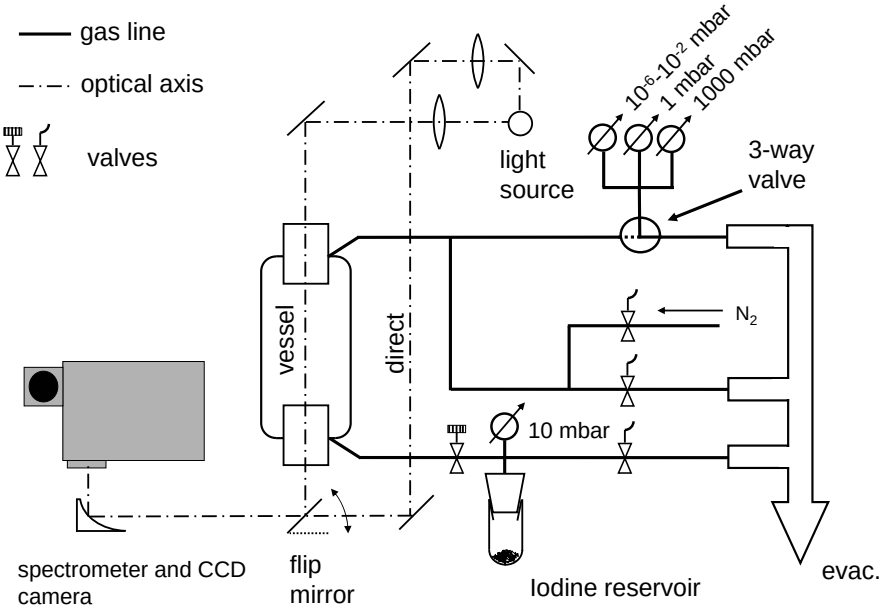

Fig. 7. In the determination of absorption cross section of I_2 simultaneous measurements of OD and pressure were used. Absorption spectroscopy was performed with a Xenon lamp, a spectrometer and CCD camera. A flip mirror enabled near-real time light source monitoring. Pressure in the vessel was automatically monitored with a 0.001 to 1.0 mbar capacitance barometer.

atmosphere. Furthermore they were recorded under spectroscopic conditions which are typical for currently used DOAS configurations. Both spectra are available as supplementary data to this publication (http://www.atmos-chem-phys.net/6/2177/2006/acp-6-2177-2006-supplement.zip).

6 Absorption cross section of I_2 at 500 nm

6.1 Experimental set-up

A schematic diagram of the set-up is shown in Fig. 7. It comprises a reaction vessel, a grating spectrometer, and a CCD camera (charge-coupled device) as detection system. The reaction vessel is made of glass and has no thermal insulation or stabilisation. Experiments were performed at room temperature. The length of the vessel was (26.4±0.2)cm. This was the shortest vessel available, thus enabling higher iodine concentrations without too large optical densities. Larger concentrations enabled more accurate measurement of pressure. To avoid I_2 condensation, the partial pressure was always kept below saturated vapour pressure. The optical windows of the vessel are made from fused silica (50 mm dia). A 150W Xenon arc lamp (Hamamatsu) was used as light source for absorption spectroscopy. After having traversed the vessel, the analysis light was directed into a Czerny-Turner spectrometer (Acton Research, 500 mm focal length) operated alternatively with one of three different gratings (1200 grooves·mm^{-1} holographic, 300 grooves·mm^{-1} and 150 grooves·mm^{-1}, both blazed at 300 nm). As resolution is not an issue for the determination of absolute absorption cross section in the continuum range at 500 nm, the measurements were performed with the 150 grooves·mm^{-1} grating (0.32 nm/pix, 0.58 nm FWHM at 25 μm entrance slit), which provides the largest intensity signals. Spectra were recorded with a CCD camera (Roper Scientific) with a 1024×1024 silicon detector chip (0.26 μm pixel width, SiTE). To enable monitoring of the light source during absorption measurements and thus to account for possible light source drift, a second beam of light was passed parallel to the vessel. With a flip mirror the light was directed either via the vessel or directly from the light source towards the spectrometer. Pressure in the vessel was the crucial parameter in the determination of concentration. Therefore it was measured using a temperature stabilised capacitance pressure transducer (MKS Baratron 627 B) with 0.001 to 1 mbar range, allowing for high linearity, low hysteresis and reproducibility of the pressure readings (specified ±0.12% of reading). For recording spectra at atmospheric pressure a capacitance pressure transducer of 1100 mbar maximum range was also connected. Zero point correction was performed with a Penning type pressure head (Edwards, 10^{-3} to 10^{-7} mbar).The temperature of the gas in the vessel, ambient temperature and the temperature of the reservoir were all measured with calibrated 3 wire Pt 100 temperature sensors. The manufacturer's specification for the sensors is ±0.07 K. The transducers were calibrated and specified to the same accuracy of ±0.07 K. As a conservative error estimate for temperature measurement ±0.5 K was assumed based on a comparative measurement. The vessel was connected to a reservoir, where the iodine was maintained. The pressure in the reser-

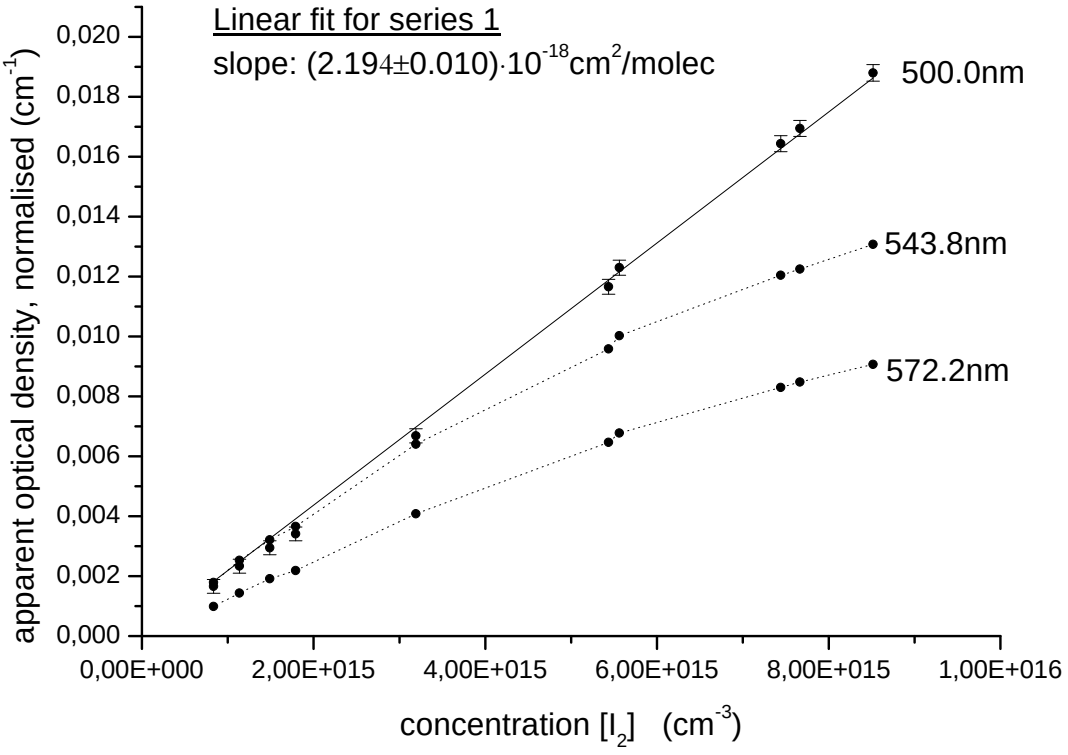

Fig. 8. The absorption cross section of I_2 at 500 nm (air) was determined by simultaneous spectroscopic and pressure/temperature measurement. For one series of measurements the linear fit of OD (normalised to unit path length) against concentration is shown, which produces the estimate for σ_{I2}(500 nm). Data for two other wavelengths from the ro-vibronic region (λ>500 nm) is shown, demonstrating the non-linear behaviour of apparent OD in that region due to resolution issues.

voir was monitored with the same type of temperature stabilised and high accuracy capacitance pressure transducer as the one connected to the vessel, but with 0.01 to 10 mbar range. Pressure heads, vessel and iodine reservoir were connected to the vacuum pump such that all could be evacuated independently of each other. During all experiments pressure and temperature readings from all sensors were automatically recorded in sufficiently short time intervals to cover all changes accurately. The I_2, resublimed p.a., was obtained from ACROS Organics, C.A.S No.:7553-56-2.

6.2 Determination of the absorption cross section of I_2

The absorption cross section was determined by simultaneously determining optical density via spectroscopic measurement and concentration via pressure and temperature measurement including careful leak rate correction.

6.2.1 Spectroscopic measurements

Each spectroscopic measurement consisted of a recording of the detector's dark signal, followed by repeated alternating measurements of the light source directly and through the vessel respectively. "Vessel" measurement and "direct" measurement consisted each of a fixed number of accumulations. By this alternating procedure a near-simultaneous recording of both was achieved which enabled a highly effective correction of possible light source drift. Prior to each measurement series the accuracy of drift correction was verified by a set of such measurements without gas in the vessel. In a preparatory experiment over half an hour a light source drift occurred with a trend of the order of 0.02/h to 0.03/h plus irregular scatter of $\pm$0.005, all in units of optical density. The drift was deliberately forced by irregularly venting the xenon arc lamp to create "worst case condition" for this test. By the described near real-time monitoring the long term drift could in all test measurements be corrected except for an irregular scatter in the averaged optical densities of less than $\pm$0.0025 in units of optical density (determined as the standard deviation across a corrected measurement of zero optical density). "Coloured" structures in the uncorrected optical density spectra of empty vessel measurements, which were caused by light source drift (i.e. deviations from the expected gaussian white noise of an ideal empty vessel measurement free of drift) were to a high degree but not completely removed. The remaining systematic error from drift was conservatively estimated to $\pm$0.006. The error of an original measurement was estimated in the sense of a maximum error as the sum of the standard deviation of a corrected empty

vessel measurement ($\pm$0.0025) plus the estimated remaining error from drift ($\pm$0.006) yielding $\pm$0.0085. All reference – i.e. empty vessel – and absorption measurements – with I_2 – were performed in this way. It is pointed out that accumulation of deposit on the vessel windows is not corrected by this approach. This is taken into account below.

Wavelength calibration was obtained from measurements of a mercury cadmium line source. Only isolated lines were used for wavelength calibration. Unresolved groups of neighbouring lines were rejected. Wavelength with respect to the 500 nm absorption cross section of I_2 is given in air. Note: Spectra in the previous section are given in vacuum wavelength for direct comparability with FTS (and other) spectroscopic measurements.

6.2.2 I_2-handling and measurement procedure

The leak rates of the empty reservoir and the vessel were determined to be 0.3 μbar·min^{-1} and 2.1 μbar·min^{-1} respectively. In both cases the increase of pressure with time, which was caused by the leak rate, displayed a clear linear behaviour on the time scale of our measurements. A linear fit to the vessel's pressure readings covering a 4 h leak test resulted in a correlation coefficient of R^2=0.99998 justifying linear extrapolation of the leak rate on the time scale of our measurements.

Prior to each filling both the vessel and the I_2-reservoir containing solid I_2 were evacuated separately to remove any foreign gases. Then the reservoir was closed to allow the build-up of gas phase I_2. The vessel was also closed and a number of spectroscopic reference measurements (each a set of vessel and direct intensity measurements) were performed on the evacuated vessel, providing the error estimate for the spectroscopic measurements and also the empty vessel reference for the determination of OD. Parallel to that the pressure in the vessel was monitored to check the leak rate of the vessel.

In the next step the I_2-reservoir was connected to allow the I_2-vapour to stream into the vessel. In general the filling proceeded initially through a fast burst resulting from the pressure gradient between the I_2-filled reservoir and the evacuated vessel. After that, filling proceeded much slower dominated by the release of I_2 from solid to gas phase in the reservoir, where the I_2 vapour was no longer in equilibrium with the solid phase. In the measurements the vessel was preferably filled using the fast initial burst. This assured that partial pressure of I_2 was always below the saturated vapour pressure and condensation of I_2 thereby minimised.

After filling, the reservoir was disconnected from the vessel and a number of simultaneous pressure readings and spectroscopic measurements were recorded. This filling and measurement procedure was repeated in several steps each time adding some more I_2 into the vessel to collect data for different concentrations. Overall pressures in the vessel were always below 0.7 mbar and well within the range of the 0.001 to 1 mbar pressure transducer. Partial pressure of I_2 was obtained by correcting the time series of overall pressures for leak rate. The simultaneous temperature measurements enabled conversion to concentration. The partial pressure of I_2 in the vessel was always below 0.35 mbar. The vapour pressure of I_2 at 298 K is 0.40 mbar (Chase 1998). Condensation on surfaces and windows was thereby minimised.

7 Analysis

In spite of the partial pressure of I_2 being below saturated vapour pressure, still wall loss of I_2 occurred in the vessel. It led to a slow but visible reduction of both partial pressure of I_2 as well as of optical density in the spectroscopic measurement. The latter covered the spectral range from 340 to 660 nm including the whole visible absorption spectrum of I_2. The correlation between both effects was high. Therefore wall loss is automatically compensated in our determination of σ_{I_2}. However, the built-up of deposit on the windows was spectroscopically observed. The absorptions of gas phase I_2 and deposit were separated by multiple multivariate linear regression of the observed time series of spectra. In this regression two observed time profiles were used as coefficients, the first of which contains dominantly the deposit's absorption (340 nm to 380 nm, averaged) and the second containing I_2 observed at 500 nm. This approach produced two continuous, smooth and non-negative separated spectra of I_2 and deposit. The fit proved the contribution of deposit at 500 nm to be negligible, while becoming increasingly important from 485 nm (worst case: 3% relative to optical density of I_2) to the blue side of the spectrum (20% at 460 nm). Consequently the recordings at 500 nm can be safely regarded as free of deposit within less than 1% relative to the I_2 absorption. Furthermore, at and below 500 nm the spectrum of I_2 is smooth and free of rotational structure. OD calculated from the pixel outputs is free of instrumental artefacts related to resolution issues and should therefore vary linearly with partial pressure, i.e. concentration of I_2. OD measured at 500 nm was plotted as a function of concentration. A linear fit with zero intercept yielded the cross section σ_{I_2} at 500 nm as the slope of the obtained line.

8 Results for the absorption cross section of I_2

Figure 8 shows the obtained OD of one of the two measurement series as a function of concentration and the corresponding linear fit. OD is normalised to unit path length. Each data point is the average of 4 to 6 individual spectroscopic determinations of optical density recorded at a certain I_2 partial pressure. Each spectroscopic determination is the average of 50 individual accumulations of "vessel" and "direct" as described above. The high quality of both linear fits for the two series is expressed by correlation coefficients of R^2=0.99951 and 0.99846 respectively. The uncertainty of

Table 2. Comparison of results for the absorption cross section of I_2 at λ=500 nm. The average was obtained by using the inverse squared error of each individual measurement as a weight. The error was determined by error propagation.

σ_{I_2}(500 nm) (10^{-18}cm^2)	method	
2.20±0.07	vapour pressure	Tellinghuisen (1973)
2.29±0.27	vapour pressure	Saiz-Lopez et al. (2004)
2.25±0.09	independent	Bauer et al. (2004)
2.18_6±0.02_1	independent	this work
2.19_1±0.02		weighted average

concentration (abscissa) was determined after correction of all systematic effects covered by measurement, i.e. leak rate and temperature drift. It therefore contains only the uncertainties of the pressure head and the temperature sensor as stated by the manufacturers after error-propagation. The uncertainty of optical density (ordinate) is based on the aforementioned maximum uncertainty of 0.0085 in units of optical density and that of the measured length of the vessel of (26.4±0.2) cm. Note that the uncertainty of 0.0085 is not yet normalised to unit path length. In the linear regression the estimated uncertainties of both axes were taken into account in the determination of the linear fit parameters and their error estimates (Press et al., 1986: Chapt. 15.3). The error estimate of the obtained cross section therefore contains both the uncertainty of the observational data (pressure and OD) and the scatter of the individual data points with respect to the linear fit. The results for the cross section σ_{I_2}(500 nm) obtained from the two series of data are $(2.19_4\pm0.01_0)\cdot10^{-18}$ cm^2 and $(2.15_8\pm0.01_8)\cdot10^{-18}$ cm^2 (Results are stated with the relevant number of significant decimal places plus an additional one – reduced in size – to minimise round-off errors in future use of the data). Using the inverse squared error as weight, a weighted average was calculated, the error of which being determined by error propagation. This yields $(2.18_6\pm0.00_9)\cdot10^{-18}$ cm^2. The uncertainty in wavelength calibration was converted to an uncertainty of absorption cross section via the derivative of the spectrum at 500 nm. Assuming an uncertainty of one pixel in wavelength calibration the uncertainty in cross section amounts to ±0.012 cm^2, which is again conservative, as the accuracy of wavelength calibration is of sub-pixel order. The final uncertainty of the cross section in the sense of a maximum error estimate is obtained by adding the uncertainty obtained from the linear regression and that from wavelength uncertainty yielding the final result of our experiments to be $\sigma_{I_2}(500\,\text{nm})=(2.18_6\pm0.02_1)\cdot10^{-18}$ cm^2.

9 Discussion

The absorption cross section determined in this way is an original determination of cross section being independent of vapour pressure data. It agrees very well with the recently published results, which are shown in Table 2. The disagreement between different data is always well within the stated uncertainties. The determination of Bauer et al. was also independent of vapour pressure using an approach similar to ours. The careful and extensive study by Tellinghuisen used vapour pressure data by Stule (1961) and Shirley and Giauque (1959). Light source drift was compensated by a two beam optical arrangement with beam alternator. The study by Saiz-Lopez et al. also used vapour pressure reference data, which they measured independently and which agrees well with the previously published data (Chase 1998, Shirley and Giauque 1959). Based on the results listed in Table 2a weighted average was calculated, which used the reciprocal squared errors of the individual results as weights:

$\sigma_{I_2}(500\,\text{nm})=(2.19_1\pm0.02)\cdot10^{-18}$ cm^2

The error of the weighted mean was determined by error propagation. Stated is a 1σ-error.

10 Conclusions

In the context of atmospheric DOAS measurements of I_2 the effect of different column density in reference spectrum and atmospheric spectrum was studied. Used was the rovibronic spectrum of I_2 in the range of 540 nm to 580 nm. For different typical DOAS configurations the systematic error was estimated, which results from using a high column density laboratory spectrum as reference spectrum for DOAS retrieval of low atmospheric column densities. The errors were found to depend in first place on limited resolution, i.e. large FWHM and only in second place on bin-size defined by grating and pixel size. For a 1200 grooves·mm^{-1} grating and 0.175 nm (close to the conditions in Saiz-Lopez and Plane 2004) the effect proved to be minor at 2%. But for spectroscopic conditions, in which for other reasons FWHM is chosen to be larger at 1.0 nm and above (see Roscoe et al., 1999), it is non-negligible, leading to an overestimation of atmospheric I_2 column density of the order of 12 to 13%. For two typical DOAS spectroscopic configurations reference spectra were dedicatedly measured at low column densities similar to atmospheric values and with typical DOAS instrumental conditions. The spectra are available as supplementary data (http://www.atmos-chem-phys.net/6/2177/2006/acp-6-2177-2006-supplement.zip). For low pressure measurements overestimation of column density was found to reach as much as 45%. Use of DOAS in low pressure laboratory studies therefore requires great care in selecting or determining appropriate reference spectra.

The absolute absorption cross section of I_2 at 500 nm in the continuum region was determined

in an independent measurement. The result of $\sigma_{I_2}(500\,\mathrm{nm})=(2.18_6\pm0.02_1)\cdot10^{-18}\,\mathrm{cm}^2$ agrees very well with previously published data and the uncertainty could be reduced by more than 50%. A weighted average of $\sigma_{I_2}(500\,\mathrm{nm})=(2.19_1\pm0.02)\cdot10^{-18}\,\mathrm{cm}^2$ of the recent determinations is suggested as the best available estimate for the absorption cross section.

Acknowledgement. This work was partially funded by the German Space Agency DLR through its support of the SCIAMACHY project, the European Union, and by the University and the State of Bremen. This work is part of and facilitated by IGBP-IGAC and EU-ACCENT Net work of Excellence. The authors wish to express their gratitude to J. Tellinghuisen for fruitful discussion and helpful suggestions after critical reading of our manuscript. The authors also want to thank A. Saiz-Lopez for helpful comments and suggestions.

Edited by: A. Hofzumahaus

References

Alliwell, S. R. and Jones, R. L. : Measurement of atmospheric NO_3 1. Improved removal of water vapour absorption features in the analysis for NO_3, Geophys. Res. Lett., 23, 2585–2588, 1996.

Bauer, D., Ingham, T., and Crowley , J. N. : Interactive comment on "Absolute absorption cross section and photolysis rate of I_2" by A. Saiz-Lopez et al., Atmos. Chem. Phys. Discuss., 4, S741–S743, 2004.

Bergland, G. D.: A guided tour of the fast Fourier transform, IEEE Spectrum, 7, 41–52, 1969.

Chase Jr., M. W.: NIST JANAF Thermodynamical Tables, 4th edition, J. Phys. Chem. Reference, Monograph 9, 1998.

Finlayson-Pitts, B. and Pitts, Jr., J. N.: Chemistry of the Upper and Lower Atmosphere, Academic Press, New York, 2000.

Gray, R. I., Luckett, K. M., and Tellinghuisen, J. : Component Analysis of the Visible Absorption Spectra of I_2 and Br_2 in Inert Solvents: Critique of Band Decomposition by Least-Squares Fitting, J. Phys. Chem. A, 105, 11 183–11 191, 2001.

Gerstenkorn, S. and Luc, P. : Atlas du spectre d'absorption de la molecule d'iode: 15 600–17 600 cm^{-1}, Laboratoire Aimé Cotton, CNRS II, 91 405 Orsay, France, 1977a.

Gerstenkorn, S. and Luc, P.: Atlas du spectre d'absorption de la molecule d'iode: 17 500–20 000 cm^{-1}, Laboratoire Aimé Cotton, CNRS II, 91 405 Orsay, France, 1977b.

Gerstenkorn, S. and Luc, P.: Atlas du spectre d'absorption de la molecule d'iode: 14 000–15 600 cm^{-1}, Laboratoire Aimé Cotton, CNRS II, 91 405 Orsay, France, 1978.

Gerstenkorn, S., Verges, J., and Chevillard, J.: Atlas du spectre d'absorption de la molecule d'iode: 11 000–14 000 cm^{-1}, Laboratoire Aimé Cotton, CNRS II, 91 405 Orsay, France, 1982.

Kato, H., et al.: Doppler-Free High Resolution Spectral Atlas of Iodine Molecule, Japan Society for the Promotion of Science, 2000.

Kortüm, G. and Friedheim, G.: Lichtabsorption und Molekularzustand des Jods als Dampf und Lösung, Zeitschrift für Naturforschung, 2a, 20–27, 1947.

Marcy, G. W. and Butler R. P. : Precise Doppler Shifts using an Iodine Cell PASP, 104, 270–277, 1992.

Ogryzlo, E. A. and Thomas, G. E.: Pressure Dependence of the Visible Absorption Bands of Molecular Iodine, J. Mol. Spectrosc., 17, 198–202, 1965.

Perner, D. and Platt, U.: Detection of nitrous acid in the atmosphere by differential optical absorption, Geophys. Res. Lett., 6, 917–920, 1979.

Press, W. H., Flannery, B. P., Teukolsky, S. A., and Vetterling, W. T.: Numerical Recipes in C: The Art of Scientific Computing, Cambridge University Press, Cambridge, U.K, 1986.

Rabinowitch, E. and Wood, W. C.: The extinction coefficients of iodine and other halogens, Trans. Faraday Soc., 32, 540–546, 1936.

Richter, A.: Absorptionsspektroskopische Messungen stratosphärischer Spurengase über Bremen, 53° N., Cuvillier Verlag, Göttingen, Germany, 1997.

Roscoe, H. K., et al.: Slant Column Measurements of O_3 ad NO_2 during the NDSC Intercomparison of Zenith-Sky UV-Visible Spectrometers in June 1996, J. Atm. Chem., 2, 281–314, 1999.

Rothman, L. S., Jacquemart, D., Barbe, A., Chris, D., Benner, M., Birk, L. R., Brown, Carleer, M. R., Chackerian, Jr., C., Chance, K., Coudert, L. H., Dana, V., Devi, V. M., Flaud, J.-M., Gamache, R. R., Goldman, A., Hartmann, J.-M., Jucks, K. W., Maki, A., Mandin, G., Massie, J.-Y, Orphal, S. T., Perrin, J. A., Rinsland, C. P., Smith, M., Tennyson, A. H., Tolchenov, J.,Toth, R. N., Vander, R. A., Auwera, J., Varanasi, P., and Wagner, G.: The HITRAN 2004 molecular spectroscopic database, J. Quantitative Spectroscopy & Radiative Transfer, 96, 139–204, 2004.

Saiz-Lopez, A. and Plane, J. M. C.: Novel iodine chemistry in the marine boundary layer, Geophys. Res. Lett., 31, L04112, doi:10.1029/2003GL019215, 2004.

Saiz-Lopez, A., Saunders, R. W., Joseph, D. M., Ashworth, S. H., and Plane, J. M. C.: Absolute absorption cross section and photolysis rate of I_2, Atmos. Chem. Phys., 4, 1443–1450, 2004, mboxhttp://www.atmos-chem-phys.net/4/1443/2004/.

Shirley, D. A. and Giauque, W. F.: The entropy of Iodine, Heat Capacity from 13 to 327 K, Heat of Sublimation, J. Am. Chem. Soc., 81, 4778–4779, 1959.

Solomon, S., Schmeltekopf, A. L., and Sanders ,W. R.: On the interpretation of zenith sky absorption measurements, J. Geophys. Res., 92, 8311–8319, 1987.

Stule, D. R. (Ed.): Thermochemical Tables, Dow Chemical, Midland, Mich., USA, 1961.

Sulzer, P. and K. Wieland : Intensitätsverteilung eines kontinuierlichen Absorptionsspektrums in Abhängigkeit von Temperatur und Wellenzahl, Helv. Phys. Acta , 25, 653–676, 1952.

Tellinghuisen, J.: Resolution of the visible-infrared absorption spectrum of I_2 into three contributing transitions, J. Chem. Phys., 58, 2821–2834, 1973.

Vogt and Koenigsberger:Beobachtungen über Absorption in Joddampf und anderen Dämpfen, Zeitschrift für Physik, 13, 292–311, 1923.